Geomorphology 381 (2021) 107661

Contents lists available at ScienceDirect

Geomorphology

journal homepage: www.elsevier.com/locate/geomorph

Probabilistic identification of rockfall source areas at regional scale in El Hierro (Canary Islands, Spain)

Mauro Rossi [a,*], Roberto Sarro [b], Paola Reichenbach [a], Rosa María Mateos [c]

[a] Istituto di Ricerca per la Protezione Idrogeologica, Consiglio Nazionale delle Ricerche, Via Madonna Alta 126, 06128 Perugia, Italy
[b] Geological Survey of Spain, Ríos Rosas 23, 28003, Madrid, Spain
[c] Geological Survey of Spain. Urb. Alcázar del Genil. Edificio Zulema, bajos, 18010 Granada, Spain

ARTICLE INFO

Article history:
Received 20 May 2020
Received in revised form 27 January 2021
Accepted 14 February 2021
Available online 20 February 2021

Keywords:
Rockfall source area
Probabilistic approach
Statistical models

ABSTRACT

Modelling rockfall phenomena is complex and requires various inputs, including an accurate location of the source areas. Source areas are controlled by geomorphological, geological, or other geo-environmental factors and may largely influence the results of the modelling. In the Canary Islands, rockfalls are extremely common and pose a major threat to society, costing lives, disrupting infrastructure, and destroying livelihoods. In 2011, the volcanic event on the island of El Hierro triggered numerous rockfalls that affected strategic infrastructures, with a substantial impact on the local population. During the emergency, the efforts performed to map the source areas and to model the rockfalls in the considerably steep landscape characterising the island were not trivial. To better identify the rockfall source areas, we propose a probabilistic modelling framework that applies a combination of multiple statistical models using the source area locations mapped in the field as the dependent variable and a set of thematic data as independent variables. The models use as input morphometric parameters derived from the Digital Elevation Model and lithological data as an expression of the mechanical behaviour of the rocks. The analysis of different training and validation scenarios allowed us to test the model sensitivity to the input data, select the optimal model training configuration, and evaluate the model applicability outside the training areas. The final map obtained from the model for the entire island of El Hierro provides the probability of a given location being a potential source area and can be used as the input for rockfall runout simulation modelling.

1. Introduction

Rockfalls are dangerous instability phenomena that occur frequently worldwide, particularly in mountainous areas. Rockfall impacts can cause severe damage due to the high kinetic energy associated with the velocity of the falling bocks (Crosta et al., 2015; Hungr et al., 2014; Mateos et al., 2020; Sarro, 2019; Volkwein et al., 2011). Rockfalls are often described in the literature by distinguishing among different spatial features: the source area, also defined as the release or detachment area; the transport area, also defined as the propagation or transit area; and the deposition or accumulation area. Such spatial subdivision is not simple, and the identification of the source, transport, and depositional areas can be obtained only with accurate mapping (Luckman, 2013; Melzner et al., 2020). Rockfalls occur under different geo-environmental settings, controlling the stability conditions of single boulders or of a portion of the cliff/outcrop. The factors controlling the occurrence of rockfall can be broadly grouped into morphometric, lithological, structural, and vegetation-related factors (Hernández Gutiérrez et al., 2015; Jaboyedoff and Labiouse, 2011; Lambert et al., 2012; Paredes et al., 2015; Sturzenegger et al., 2007).

Under susceptible conditions, rockfalls occurrence can be determined by a variety of natural processes, acting both over short or long term. Seismic shaking/acceleration or rainfall-induced pore pressure increases can be easily recognised as short-term rockfall triggers, whereas it is more difficult to identify long-term triggers, for example, related to frost and thaw cycles or thermal rock movements and expansions (Luckman, 2013; Mateos et al., 2012).

A rockfall model does not necessarily have to be able to describe all parts of the rockfall process and the movements of boulders from the source to the deposition area, even though complete information is relevant for effective hazard management. One of the major difficulties of rockfall modelling is related to the uncertainty associated with the source area identification, and in the literature, various approaches have been utilised for this identification. Some authors have proposed direct recognition in the field (Agliardi et al., 2009) and the interpretation of aerial photographs or topographic base maps (Guzzetti et al., 2004), while others have used remote sensing techniques such as Unmanned Aerial Vehicle (UAVs) or Laser Scanning (Santangelo et al., 2019; Sarro et al., 2018). Aksoy and Ercanoglu (2006) identified source

* Corresponding author.
E-mail addresses: mauro.rossi@irpi.cnr.it (M. Rossi), r.sarro@igme.es (R. Sarro), paola.reichenbach@irpi.cnr.it (P. Reichenbach), rm.mateos@igme.es (R.M. Mateos).

https://doi.org/10.1016/j.geomorph.2021.107661

areas from field surveys combined with a rule-based fuzzy evaluation, incorporating the altitude difference, number of discontinuities, number of wedges, and number of potential slides. The most common simple morphometric approach consists of a heuristic definition of a threshold angle, above which the hillslope may be considered as unstable and potentially a rockfall source area (Corona et al., 2013; Frattini et al., 2008; Guzzetti et al., 2003; Jaboyedoff and Labiouse, 2003; Sarro et al., 2020; Toppe, 1987). The threshold angle can also be identified with more complex approaches. Loye et al. (2009) introduced a methodology that enables the detection of rockfall sources at a regional scale based on a geomorphometric analysis performed on High-Resolution DEMs (1 m cell size). Losasso et al. (2017) adopted a methodology based on the evaluation of the slope angle distribution of the main lithological unit. Muzzillo et al. (2018) considered a slope angle greater than the formation frictional angle. Fanos and Pradhan (2018) proposed a hybrid model for rockfall source identification based on the stacking ensemble model of random forest, artificial neural network, Naive Bayes, and logistic regression in addition to a Gaussian mixture model using high-resolution airborne laser scanning data (LiDAR).

In this study, we investigated a method for the identification of rockfall source areas in El Hierro, the westernmost island of the Canary Islands. Because of the steep topography and volcanic geological complexity, rockfalls in the Canary archipelago are exceptionally common and represent a major threat to society, costing lives, disrupting infrastructure, and destroying livelihoods. The focus of the study is the description of a regional approach for the identification of rockfall source areas, exploiting a combination of multiple multivariate statistical probabilistic models. In the manuscript, we first describe the study area and the available data. We then present the methodology and analyses performed for the probabilistic identification of the source areas. Finally, we discuss the results and provide concluding remarks.

2. Study area and data

The Canary Islands are a Spanish overseas territory and one of the larger volcanic archipelago. They consist of eight volcanic islands off the Atlantic coast of Morocco, aligned along a W–E direction for approximately 800 km (Fig. 1). The geological origin of the archipelago is still under debate, but in the literature, it is commonly interpreted as a hotspot track (Fullea et al., 2015). El Hierro, located at the southwestern edge of the Canary Islands (Fig. 1), has an extension of 268.71 km^2 and a population of 10,968 inhabitants (Instituto Nacional de Estadística, 2019) distributed in three municipalities: Frontera, El Pinar, and Valverde. The island has a peculiar truncated trihedral shape, with three convergent ridges of volcanic cones separated by wide horseshoe-shaped embayment (Fig. 1). The elevation reaches a maximum of 1501 m at the top of a relief formed by three overlapping seafloor volcanoes (Carracedo et al., 2001; Martí et al., 1996). At least four giant landslides (El Golfo, El Julan, San Andres, and Las Playas) have modified approximately 450 km^3 of the island during the last 200–300 thousand years, with each landslide removing approximately 3% of the total edifice volume (Gee et al., 2001). The island is located in a transitional zone between temperate and tropical climates. Higher rainfall levels are recorded during the autumn and winter, mainly in December, when heavy storms are frequent, which are associated with intense rainfall and strong winds (Bechtel, 2016).

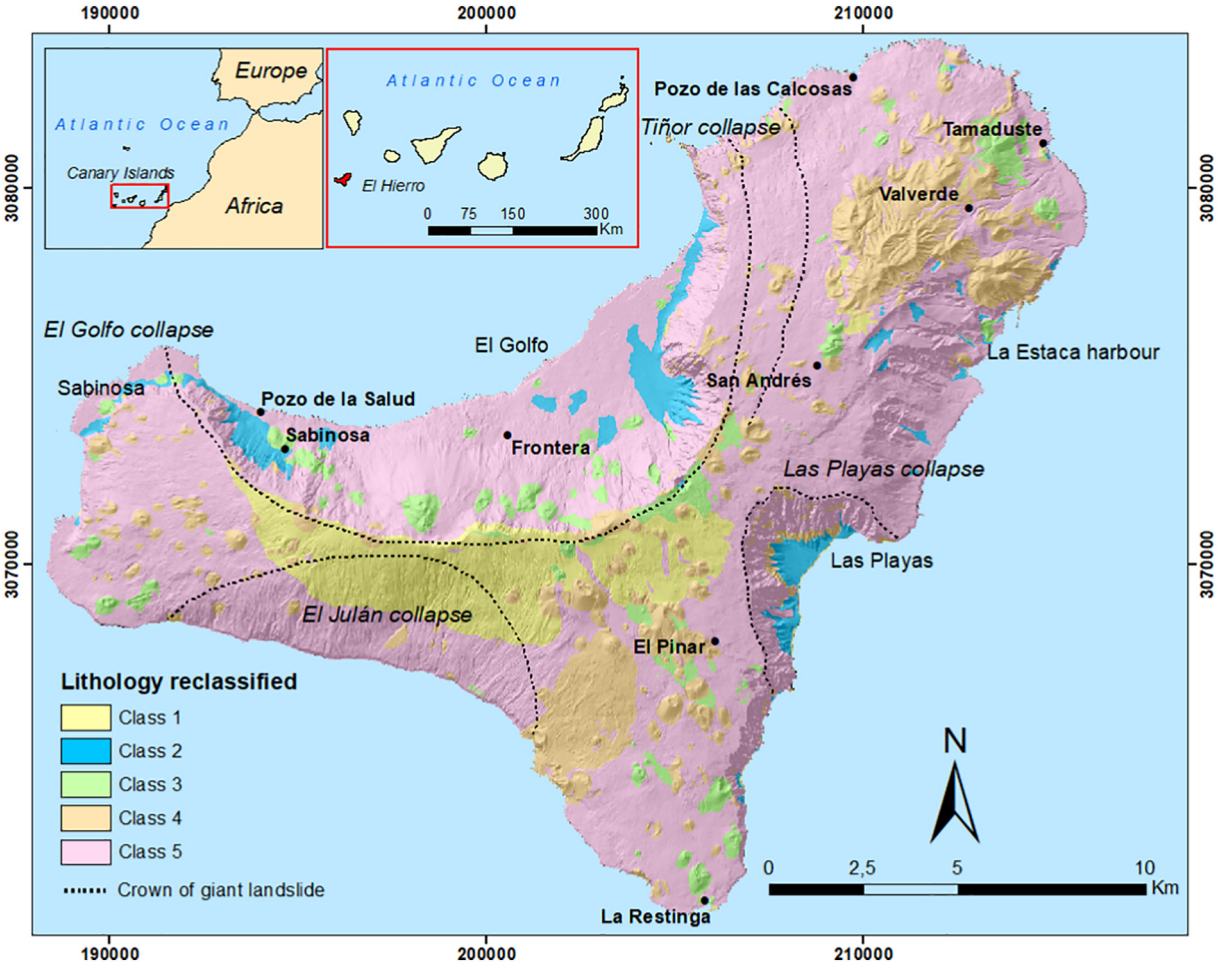

Fig. 1. Simplified lithological map of El Hierro derived from the geological map. Crowns of giant landslides shaping the island morphology are shown with dashed lines.

On the island, rockfalls are a widespread natural process, occurring generally along the steepest cliffs and forming evident talus deposits with a conical shape. The impact of rockfalls is significant, as reported by the numerous damages to structures and infrastructures. In 2011, the seismicity induced by a submarine volcanic eruption triggered numerous rockfalls, which severely affected the road network, causing substantial direct and indirect social and economic damage. During the event, field observations carried out by technicians of the Geological Survey of Spain (IGME) in the El Golfo area enabled a preliminary evaluation of the cliff stability along road HI-5, near the Roquillos tunnel. IGME highlighted a complex scenario for the analysis of rockfall hazard, particularly for the identification of rockfall source areas. Rockfall occurrences are primarily conditioned by numerous factors, such as the distribution of different volcanic materials, diversified slope gradients, and large erosion rates. In addition, the difficult accessibility to the rock massifs limited the ability to directly map the rockfall source areas in the field. One year after the seismic event, a research group at the Polytechnic University of Madrid and the Geological Survey of Spain developed a semi-quantitative heuristic methodology for the rockfall detachment susceptibility zonation of El Hierro (Fernandez-Hernández et al., 2012). The methodology is based on the overlapping of thematic maps of conditioning factors to mass movements using standard GIS procedures in order to obtain a susceptibility numerical index.

2.1. Identification of active and prone rockfall source areas

In this work, we used a combination of different techniques to identify source areas. First, we selected four test sites that are well recognised as prone to rockfalls: Las Playas, Sabinosa, El Golfo, and La Estaca harbour (Fig. 2). Then, for the test sites, we mapped the source areas using the following methods: orthophoto interpretation (Petje et al., 2005), analysis of the digital elevation model (Abellán et al., 2006; Jaboyedoff et al., 2012; Losasso et al., 2017; Loye et al., 2009), and analysis of geological and geomorphological features and field surveys (Ruiz-Carulla et al., 2015). For the sites, we were able to differentiate "active" and "prone" source areas. In the active areas, we recognised recent evidence of rockfall detachments by performing detailed mapping, which combines DEM analysis, orthophoto interpretation, field observations, UAV analysis, and the information provided by the local authorities. First, the DEM analysis allowed us to identify relevant topographical features, such as cliffs and steep slopes, successively during the field campaign in December 2018, fresh detachment areas were mapped and verified in situ with the local authorities (Road Maintenance Service). At the El Golfo test site, owing to the difficult and limited accessibility of the cliffs, UAVs were used for the recognition of active areas. The active areas are predominantly located in hard rocks, such as basalts and cemented pyroclastic deposits with slope angles over 45°–50°.

In the prone areas, we distinguished geological and geomorphological characteristics potentially prone to rockfall occurrence, without recent evidence of detachments. Prone areas were identified heuristically by analysing orthophotos in the terrains with slope angles greater than 45°. The map in Fig. 2 shows the distribution of the active and prone areas in the four test sites.

2.2. Thematic data

The investigations carried out at the four test sites (Fig. 2) allowed us to identify the geo-environmental factors characterising the cliffs, which we considered relevant for the probabilistic identification of the rockfall source areas. In the preliminary phase, we selected topography, lithology, presence of dikes, and land use/cover as the conditioning factors, with the latter excluded during the analyses because steep slopes are primarily classified as bare soil.

The topography was derived from the Digital Elevation Model (DEM) at a 5 m × 5 m resolution provided by the National Geographic Institute (http://www.ign.es/ign/main/index.do). The DEM was used to compute the morphometric information, such as slope, curvature, and aspect.

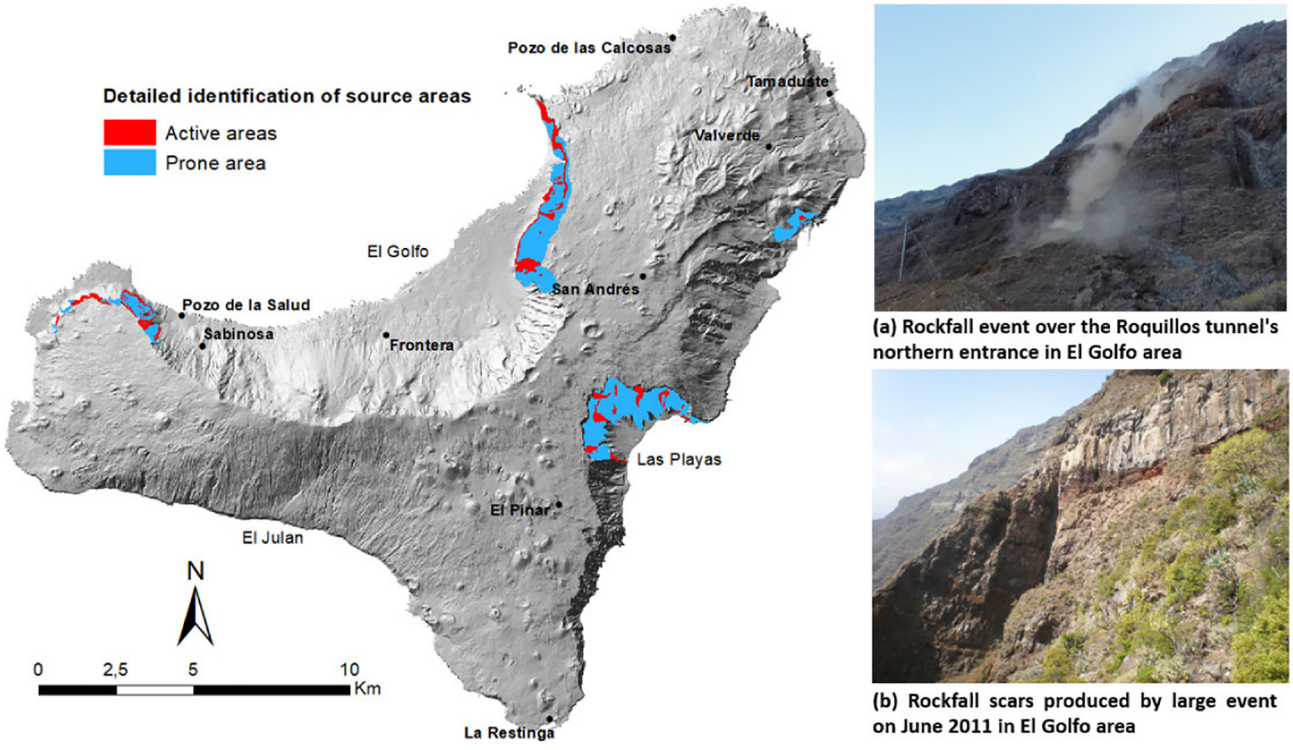

Fig. 2. Map of active and prone rockfall source areas in the 4 test sites: Las Playas, Sabinosa, El Golfo, and La Estaca harbour (Photos a and b by courtesy of José Medina Alejandro, Cabildo of El Hierro).

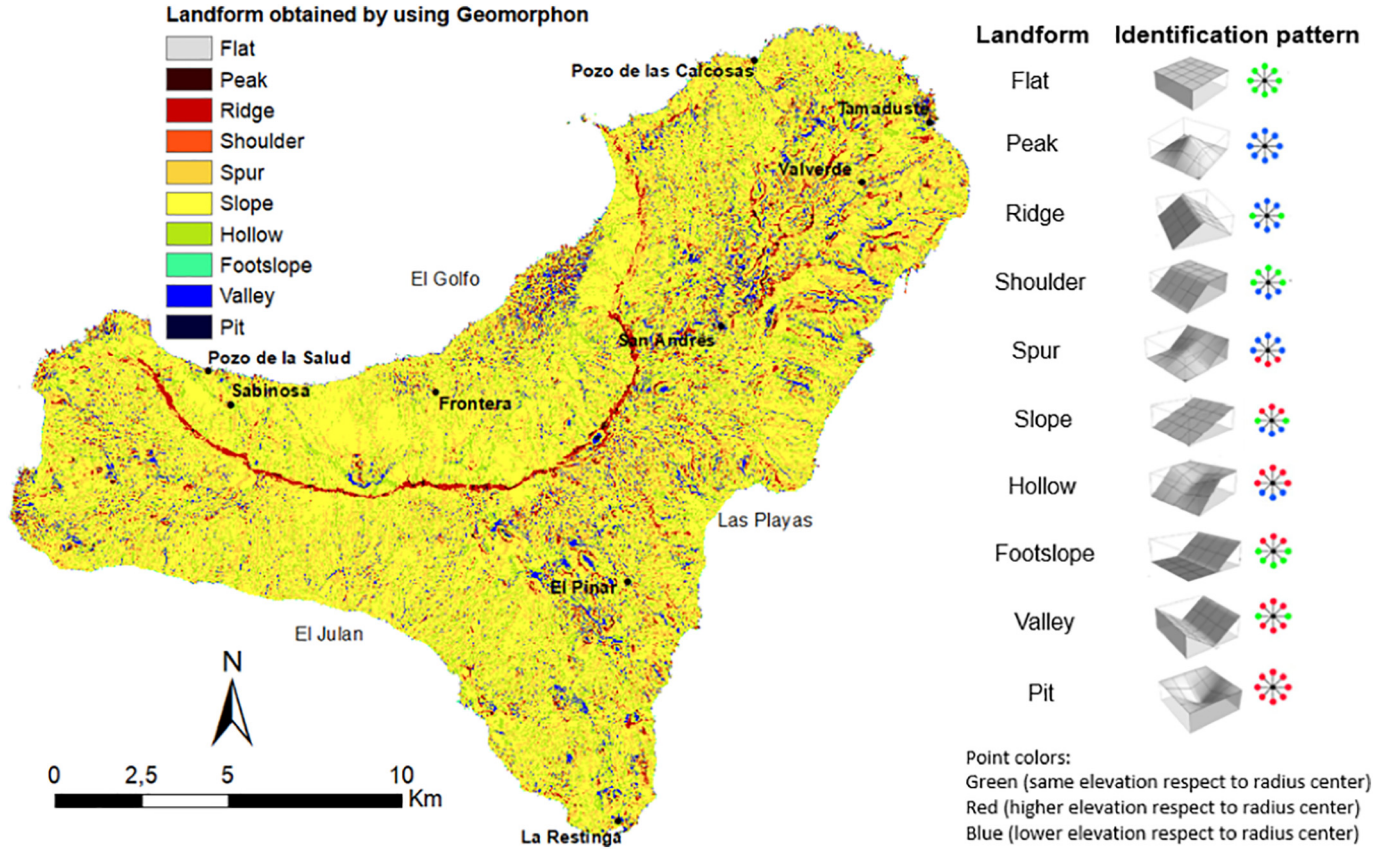

Fig. 3. Map of landforms obtained using "Geomorphon" (Jasiewicz and Stepinski, 2013). The island is divided into 10 landform types that were used to exclude flat areas, which are meaningless for source area identification.

To exclude flat areas, which are meaningless for source area identification, we performed a landform classification using the "Geomorphons" method (Jasiewicz and Stepinski, 2013). The method classifies and maps landforms from a DEM based on the principle of pattern recognition. The tool, based on the comparison of the elevation of each pixel with the values of the eight surrounding pixels, classifies the terrain into 10 landform types (Fig. 3).

The lithological information was derived from the geological map provided by the Geological Survey of Spain at a 1:25,000 scale, which shows 38 different geological units and is reclassified into five classes based on their lithological characteristics. Class 1 includes soft soils and groups the lithologies outside the source areas, such as lapilli and sand; Class 2 represents hard soils, such as sedimentary deposits (mainly conglomerate); Class 3 contains soft rocks, such as the pyroclastic material; Class 4 groups hard rocks, such as basalt flows and trachyte; and Class 5 includes very hard rocks, such as dikes, volcanic breccia, and massive basalts (Fig. 1 and Table 1).

Following the field observations, one relevant geological factor influencing the location of the rockfall source areas is the presence of dikes. In El Hierro, there is a complex dike swarm, exposed predominantly along the cliffs and the oldest ravines. Most of the dikes are subvertical (Fig. 4), trending parallel to the axis of the rift and range in thickness from 0.1 to 12.5 m (Carracedo et al., 2001). Starting from the available geological map where dikes are well recognised and mapped (Becerril et al., 2016), we prepared a raster layer showing the spatial distribution of the dikes. The dike density map with a 5 m × 5 m resolution (Fig. 4) was obtained by applying a 75-m kernel interpolation. We choose a kernel interpolator in place of a classical Kriging approach because of its better performance in applications where small datasets are available (Mühlenstädt and Kuhnt, 2011).

Table 1
Lithology classes derived from the geological map of El Hierro (adapted from Hernández-Gutierrez, 2014).

Class	Lithology	Type
1	Sand and Lapilli	Soft soils
2	Sedimentary deposit	Hard soils
3	Pyroclastic material	Soft rocks
4	Basalt flows and Trachyte	Hard rocks
5	Breccia and massive basalt	Very hard rocks

3. Probabilistic source areas modelling

For the probabilistic identification of rockfall source areas, we used a combination of multiple supervised classification models, requiring a map of the observed source areas (i.e. dependent/grouping variable) and a set of independent thematic information derived from the DEM and the geological map (i.e. explanatory variables) as inputs. The probabilistic analysis was formalised and tailored for the purpose of a tool called LAND-SUITE (LANDslide - SUsceptibility Inferential Tool Evaluator), an open source software coded in R (R Core Team, 2018), originally implemented for landslide susceptibility assessments. LAND-SUITE includes three main modules: (i) LAND-SE (LANDslide - Susceptibility Evaluation), which performs susceptibility modelling and zonation (Rossi and Reichenbach, 2016); (ii) LAND-SIP (LANDslide - Susceptibility Input Preparation), which is designed for the preparation of the inputs for LAND-SE; and (iii) LAND-SVA (LANDslide - Susceptibility Variable Analysis), which is designed for the explorative analysis of the training and validation datasets that are used as inputs for LAND-SE. The software has several advantages, including the ability to: (i) use different cartographic units (pixel-based or polygon-based); (ii) evaluate pairwise correlations and multicollinearity problems among explanatory information and to perform conditional density analysis of the input variables; (iii) perform different types of validation analyses;

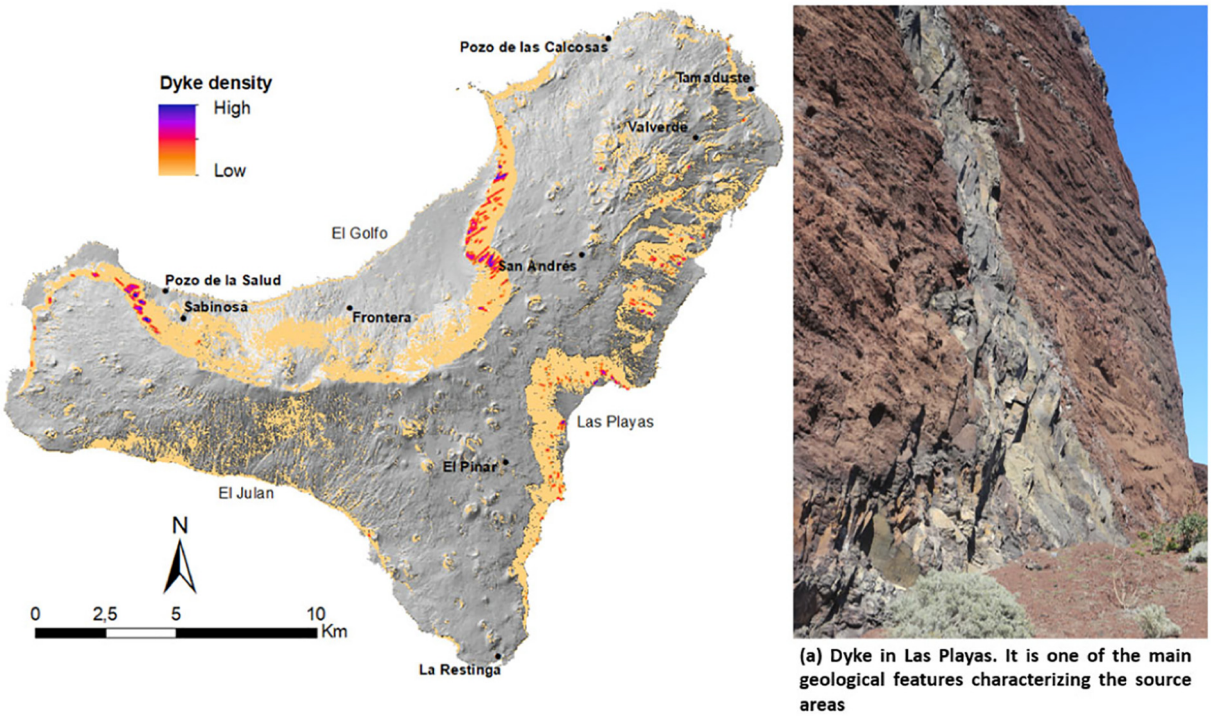

Fig. 4. Dike density map obtained applying a Kernel interpolation to the dikes shown in the geological map.

(iv) evaluate the model prediction skills and performances using success and prediction rate curves (Chung and Fabbri, 1999; Chung and Fabbri, 2003); (v) provide results in standard geographical formats (shapefiles, geotiff); (vi) perform an optimisation and stabilisation of the modelling algorithms; and (vii) utilise additional computational parameters to tune the calculation procedure for the analysis of large datasets (Rossi et al., 2010; Rossi and Reichenbach, 2016).

Probabilistic source area maps, expressing the probability of a region being a potential rockfall source area, were obtained by selecting the pixel as the mapping unit. We used the logistic regression model (LRM) integrated in the tool to analyse different training/validation scenarios, with the main purpose of evaluating the model sensitivity (i.e. model output variations that can be attributed to input variable variations) to the dependent variable selection and selecting the best training configuration to model the entire island. Conversely, the final source area zonation was performed, enabling the combination of different statistical modelling methods (i.e. linear discriminant analysis, quadratic discriminant analysis, and logistic regression model), adopting a regression-based approach. The combined model (CFM model) was prepared by applying a logistic regression and using the probabilistic outcomes of the single models as independent variables and the presence or absence of source area in the pixel as grouping variables (Rossi et al., 2010; Rossi and Reichenbach, 2016).

The probabilistic source area maps, resulting from the different model applications and configurations, were evaluated considering various outputs aimed to verify the modelling performances and to estimate the associated uncertainty. Specifically, to evaluate the probabilistic source area zonation, we accounted for the output expressing the variation of the model sensitivity, specificity, and Cohen's kappa index for the different values of the probability thresholds, ROC plot, and fourfold plot (also referred to as a contingency plot). The fourfold plot graphically summarises the number of true positives (TP), true negatives (TN), false positives (FP), and false negatives (FN) of the contingency table obtained by comparing the observed and modelled source areas (Fawcett, 2006). The ROC curve shows the "hit rate" (y-axis) vs. the "false alarm rate" (x-axis) values computed for different probabilistic thresholds. The "hit rate", also known as sensitivity or "true positive rate", is computed as TP/(TP + FN) and specifies the proportion of source areas pixels correctly predicted by the model. The "false alarm rate", also known as "false positive rate", is computed as FP/(FP + TN), and specifies the proportion of pixels out of the known source areas incorrectly predicted as source areas. The area under the ROC curve (AUC_{ROC}) is a quantitative measure of the model performance (Mason and Graham, 2002; Jolliffe and Stephenson, 2012; Fawcett, 2006). AUC_{ROC} varies between 0 and 1, with 1 representing a perfect model performance and 0.5 indicating the performance of an uninformative model.

3.1. Input data preparation

All input variables were converted to a raster format with a pixel resolution of 5 m × 5 m (i.e. the DEM resolution). In the modelling, the presence/absence of the observed source areas in the pixel was used as a dependent (i.e. grouping) variable, while the slope angle, curvature derived from the DEM, and reclassified lithology and dike density maps derived from the geological map were used as independent variables (see §2). Different procedures were used to include continuous (available as raster layers) and categorical (available as vector and raster layers) variables in the modelling. The continuous variables were directly used in the analysis, while the categorical variables were converted to numerical dummy variables, ranking the classes of each categorical layer based on their expected (i.e. heuristically defined) propensity to be a rockfall source area. The ranking of the categorical variables was verified by considering the density of the source area per class (i.e. conditional density plots produced by LAND-SVA), and in the case of mismatch, modified accordingly. The analysis of the variable pairwise correlation and multicollinearity was performed using LAND-SVA to verify the presence of collinearity problems among the independent variables. Aspect were excluded from the modelling because of the strong correlation with the slope. The final set of variables included morphometric variables (slope and curvature), lithological classes, and dike density. To verify the goodness of this set of variables, the Wald test was performed during the LRM modelling to evaluate the variables' significance (R Core Team, 2018).

Table 2
Scenarios and Cases selected for the model training and validation. The table shows the selected test sites and the value assigned to the prone areas for each scenario/case.

Scenario	Case	Selected test sites		Prone areas value	
		Training	Validation	Training	Validation
A	1	El Golfo, Las Playas	Sabinosa, La Estaca	No data	No data
	2	Sabinosa, La Estaca	El Golfo, Las Playas	No data	No data
	3	El Golfo, Las Playas Sabinosa, La Estaca	El Hierro island	No data	No data
B	1	El Golfo, Las Playas	Sabinosa, La Estaca	1	1
	2	Sabinosa, La Estaca	El Golfo, Las Playas	1	1
	3	El Golfo, Las Playas Sabinosa, La Estaca	El Hierro island	1	1
C	1	El Golfo Las Playas	Sabinosa, La Estaca	No Data	1
D	3	El Golfo, Las Playas Sabinosa, La Estaca	El Hierro island	No Data	1

All the analyses were performed using a mask to exclude the flat areas, which are meaningless for source area identification. The mask covering the entire island was obtained by selecting five landform types (i.e. ridge, shoulder, spur, slope, and hollow) obtained using the "Geomorphons" method (Fig. 3).

The probabilistic models were calibrated using an equal number of pixels in (i.e. with value equal to 1 corresponding to source area presence) and out (i.e. with value equal to 0 corresponding to source area absence) of the observed source areas. In the analyses, we constrained the random selection of pixels with a value equal to 0 (i.e. source area absence) in the vicinity of the observed source areas. This was done by establishing a 250-m buffer outside the active and prone source area polygons using standard GIS procedures. The dimension of the buffer was selected considering the distance between the top of the cliff and the maximum runout distance, which was recognised by the lower limit of alluvial fans and debris cones at the base of the escarpments. We considered the buffer areas as zones where source areas were not identified with sufficient certainty during the mapping activities, and hence, where the geomorphological setting is unlikely to be a source of rockfalls.

3.2. Model application

Using the dependent and independent variables, we prepared the probabilistic source area zonation with the associated uncertainties. To test and verify the model sensitivity to the dependent variable, we trained the model selecting different mapped source areas (i.e. active, prone, and buffer) as the grouping variable. The grouping variable was set to 1 when the pixels corresponded to mapped source areas and to zero in the opposite case. In the modelling, the source areas mapped as active were always classified as 1, buffer areas always as 0, and prone areas as 1 or No_Data depending on the different scenarios (Table 2). In the calibration/training phase, we constructed a probabilistic model relating the dependent and the independent variables, while in the validation phase, we applied the resulting model for various portions and for the entire island of El Hierro. For this purpose, we identified four scenarios (A, B, C, and D) considering several dependent variable configurations for model training and validation. For each scenario, we simulated different cases (Cases 1, 2, and 3) considering combinations of test sites as training and validation areas (Table 2). The different configurations (Table 2) were identified with the objective of testing and verifying the model sensitivity to (i) different training/validation sets and (ii) different types of data (i.e. considering only active or active and prone as source areas) used as the dependent variable to train the model.

To evaluate the sensitivity of the training and validation models, we performed different tests (hereafter denoted as cases) changing/inverting the training and the validation test site selection (Table 2). For Scenarios A and B, we considered Case 1, where two test sites (Fig. 2 and Table 2) were selected as the training set and two as validation sites, Case 2, where the training and validation test sites were switched, and Case 3 where the model was trained with the four test sites and applied over the entire island. In Scenario A, the model was trained and validated considering only active source areas (value equal to 1) and the buffer zone (value equal to 0), whereas pixels in the prone areas were not used in the analysis. In Scenario B, both the active and prone areas were used to train and validate the models (Table 2). Scenario C considers only Case 1, where the training and the validation test sites are the same as in Case 1 of Scenario A, but with a different selection of source area pixels used to validate the model (Table 2). Scenario D considers only Case 3, where the model was trained using the four test sites and the result was applied to the entire island, considering the prone areas along with the active area. Table 2 summarises the test sites and the values assigned to the prone areas for model training and validation.

The results of the source area modelling (i.e. model training and validation performances) are quantified by the values of the overall accuracy (ACC) and area under the ROC curve (AUC_{ROC}) (Table 3). The asterisks in the table highlight the results of the model applied to the entire island (i.e. model validation of Case 3), which should be considered only indicative of the real model performance. In fact, because the distribution of source areas is known only in the four surveyed test sites, the model performance metrics for the entire island may be partially biased. The minor differences existing for the same cases among the different scenarios are the results of the random procedure used to select the pixels in correspondence of the source areas (values = 1 sampled in mapped source areas) or not (values = 0 sampled in buffer areas).

This bias is not present in Cases 1 and 2, where the models were trained and validated in the surveyed test sites. Fig. 5 shows

Table 3
Accuracy and area under ROC for the 4 scenarios. The asterisk highlights the results of the models applied to the entire island, which should be considered only indicative of the real model performances.

Scenario	Case	Accuracy (ACC)			Area under Roc Curve (AUC_{ROC})		
		Training	Validation	Difference	Training	Validation	Difference
A	1	91.24	90.83	0.41	0.957	0.966	−0.009
	2	91.02	89.93	1.09	0.969	0.956	0.013
	3	91.26	90.6*	0.66*	0.961	0.966*	−0.005*
B	1	90.28	86.14	4.14	0.944	0.932	0.012
	2	86.28	90.68	−4.40	0.933	0.943	−0.01
	3	89.47	88.61*	0.86*	0.945	0.951*	−0.006*
C	1	91.24	86.43	4.81	0.957	0.932	0.025
D	3	91.28	88.60*	2.68*	0.961	0.954*	0.007*

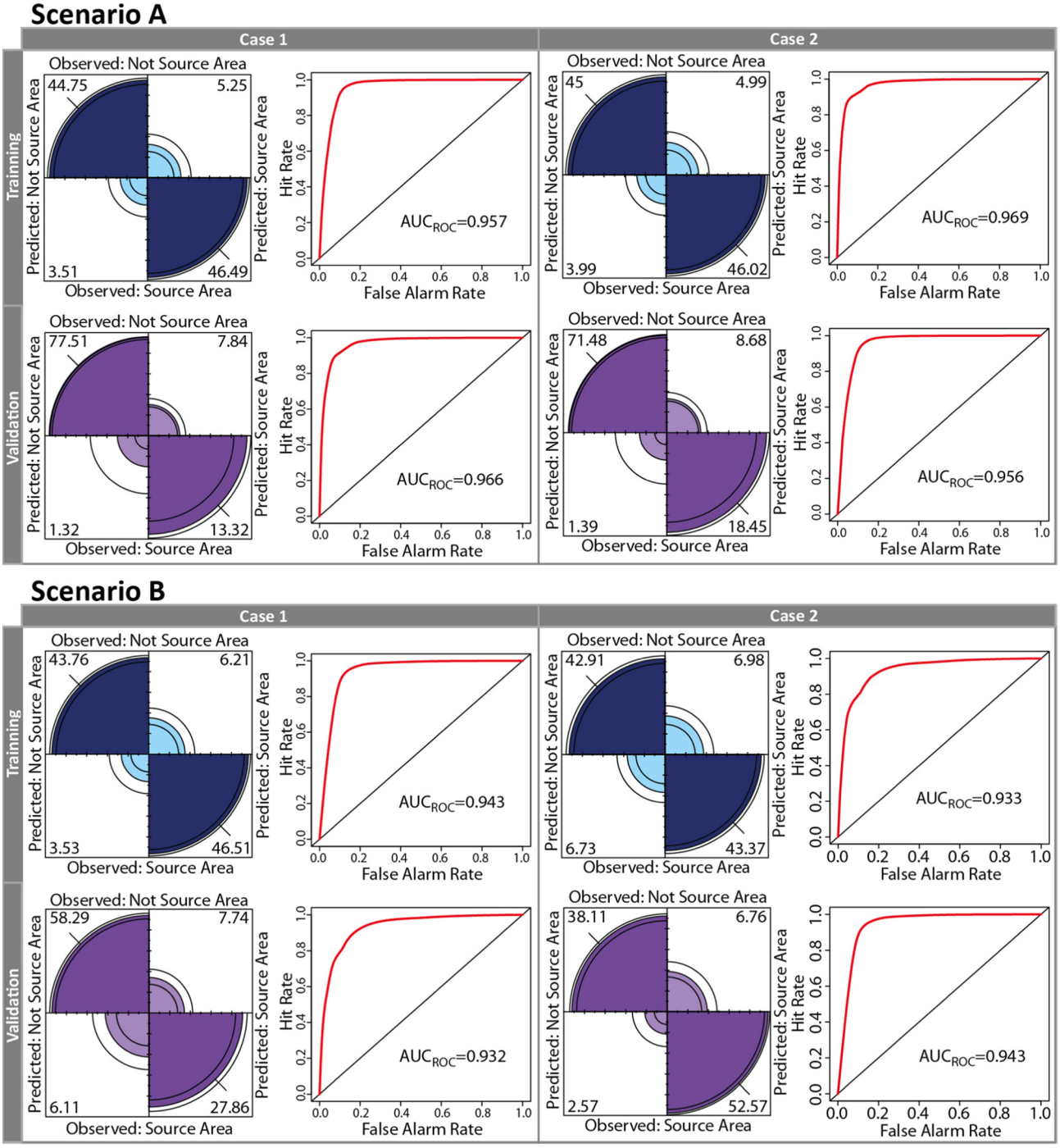

Fig. 5. Contingency and ROC plots for Cases 1 and 2 for the Scenario A and B, where the models were trained and validated in the surveyed test sites.

contingency plots (i.e. graphical representation of the contingency matrix comparing the model predictions and observations) and ROC plots obtained for Cases 1 and 2 of Scenarios A and B. Fig. 6 shows the contingency and ROC plots for Case 1 of Scenario C, where the model was trained and validated in the surveyed test sites and the prone areas were not used to train the model.

Fig. 7 illustrates the source areas maps for the entire island, obtained by training the probabilistic model with the data from the four test sites with different prone area configurations in both the training and validation phases (Case 3 for Scenario A, B, and D). The maps show the probability of each pixel being a source area, ranging from 0 (low) to 1 (high). In the figure, the contingency and the ROC plots demonstrate the training performances of the models.

4. Discussion

The identification of source areas is a key step that largely influences the results of rockfall simulations and modelling (Agliardi and Crosta, 2003). Because the position of source areas along hillslopes does not follow a completely random distribution, it cannot be predicted efficiently and effectively using simple approaches. In many cases, more comprehensive models can be used to account for the varying factors controlling rockfall initiation and source area locations.

In El Hierro, the elevation and high slope angles of the cliffs make the recognition and mapping of the source areas quite complex. For this reason, detailed identification and mapping of source areas have been limited to a few test sites (Fig. 2), where rock detachments are more

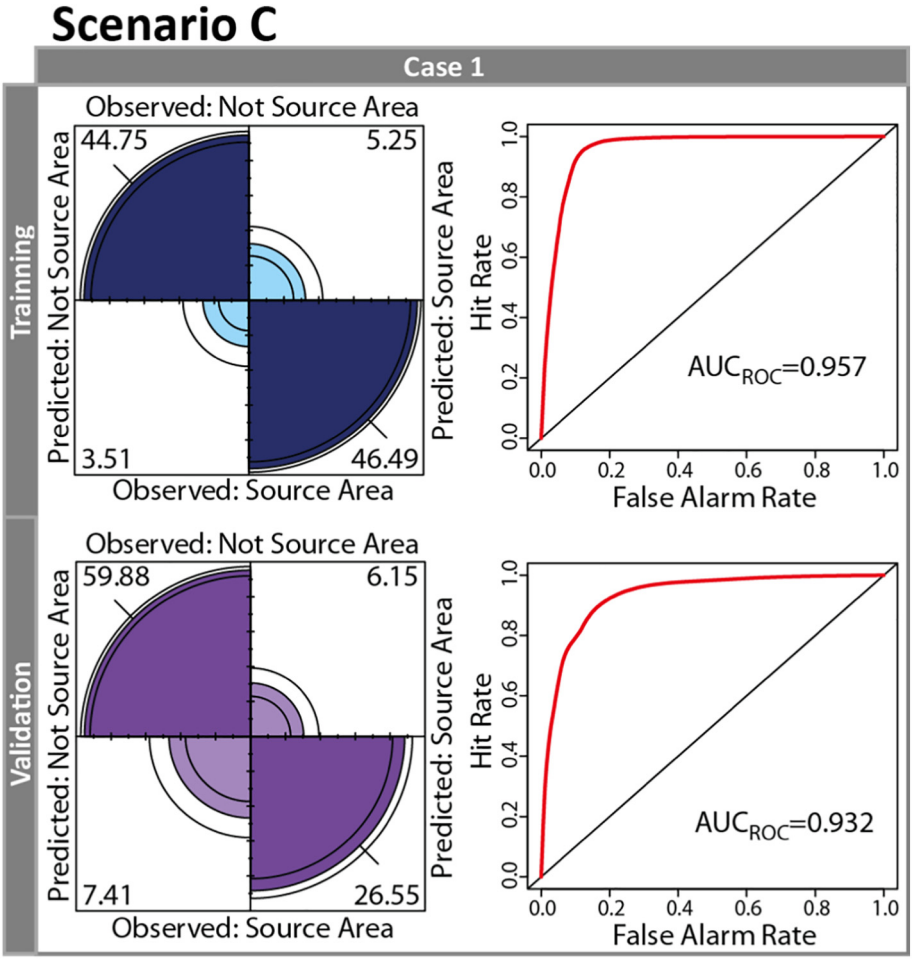

Fig. 6. Contingency and ROC plots for Case 1 for Scenario C, where the model was trained and validated in the surveyed test sites.

evident and visible. The information collected at the test sites was used to train the probabilistic models for the identification of rockfall source areas. Several training/validation model configurations were tested (Table 2) with a multifold objective: (i) testing the probabilistic model sensitivity to input data, (ii) testing the model applicability to outside the training areas, and (iii) finding an optimal training configuration to apply the model over the entire island. In the modelling, we always used the same set of independent variables that were selected with the support of the procedures implemented in LAND-SVA. The significance of the variables, computed using the Wald test, was high in all the simulations, confirming the robustness and reliability of the environmental data selected for the analysis. We consider this set of variables easy to acquire, making the approach applicable in similar volcanic settings. Overall, the analysis of the variability of the LRM model coefficients obtained for all the considered Scenarios and Cases shows that the four thematic variables were significant and positively/directly contributing to the source area identification.

The analysis of the accuracy (ACC) and AUC_{ROC} values (Table 3) revealed the good ability of the models to discriminate pixels potentially being/not-being a rockfall source area. In particular, the accuracy in both the training and validation phases is always greater than 86.14, and the AUC_{ROC} values are greater than 0.932.

In Scenario A, the model was trained and validated considering only active source areas (value equal to 1) and the buffer zone (value equal to 0), whereas pixels in the prone areas were not used in the analysis (Table 2). The results are similar for the three cases (Table 3), with minor differences among the contingency and ROC plot values for the training and validation sets (Fig. 5). The number of FP (i.e. pixels wrongly predicted as being source areas) and FN (i.e. pixels wrongly predicted as not being source areas) is considerably small in these cases. The performance of the model is especially high, both during the training and validation, even though in the validation phase, the model is only applied to active source areas and does not provide additional information on other possible critical zones (i.e. in correspondence of prone source areas). The comparison of Cases 1 and 2 indicates that the model is slightly influenced (i.e. small differences between training performances) by the location of the test sites selected for training (Table 2) and additionally highlights that the model exportability outside the training areas is high (i.e. small differences between training and validation performances). Case 3, which applies the model trained on the four test sites to the entire island, is slightly better compared with the other two cases.

In Scenario B, where the test site configurations are the same as in Scenario A, both the active and prone areas were used to train and validate the models (Table 2). The analysis of the contingency plots (Fig. 5) and accuracy values (Table 3) reveals a difference of approximately 5% between Case 1 and Case 2 from training to validation, whereas the difference in the AUC_{ROC} values is small. Unlike Scenario A, selecting different test sites in training may lead to appreciable differences.

The comparison of the evaluation metrics for Scenarios A and B demonstrates that the models benefit from the use of only active source areas in both the training and validation phases (Table 3 and Fig. 5).

Scenario C tests the ability of the model trained using only active areas to predict the prone source areas in validation. As expected, the model training performance metrics are similar to those obtained in Scenario A with similar training, but with reduced validation performances. This

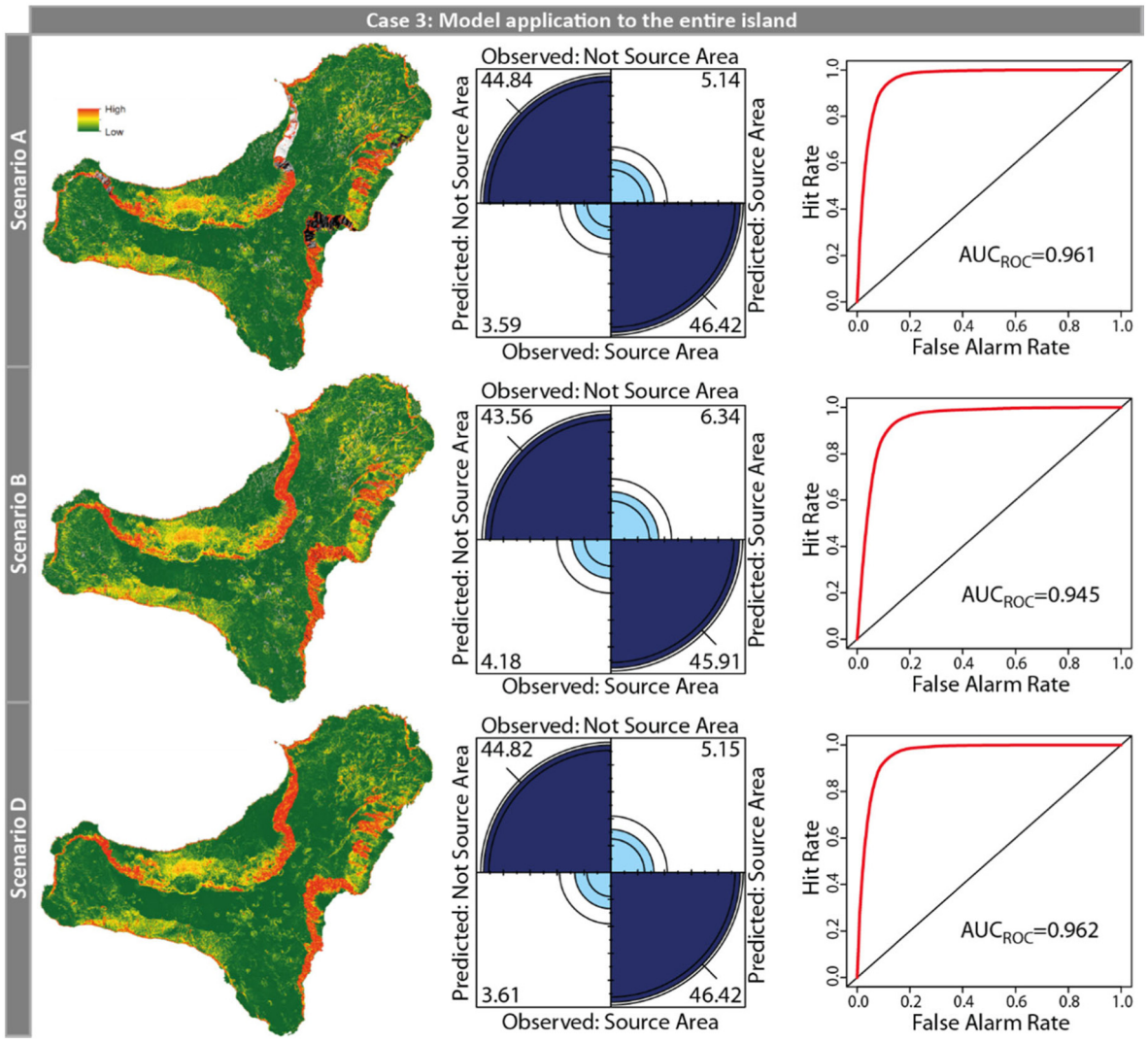

Fig. 7. Probabilistic source areas maps obtained applying different model training configurations to the entire island (Case 3). The maps show the probability of the pixels being a source area, ranging from 0 (low) to 1 (high). Contingency and ROC plots show model training performances.

suggests that the model is sensitive to the selection of source area types and highlights that active and prone area features represent distinct source area conditions. In particular, prone areas provide a less accurate characterisation of the conditions leading to rockfall initiation. This can be related to the methods used to map prone areas that are based on a more heuristic inference. Nevertheless, we maintain that this type of mapping could be applicable for preliminary modelling applications.

In Scenario D, the model was trained in all four test sites using only active source areas (Table 2) and was applied to the entire island using as a benchmark for both source area types. Inspection of the contingency plots (Fig. 5) reveals that the training correctly predicted 91.24% of the pixels as source areas or not. As expected, the ROC curves and relative AUC_{ROC} values also indicate better prediction skills than in Scenario B.

Overall, the results demonstrate that the models are sensitive to the type of source areas used in the training phase, with the best performances obtained with the active areas. The performances of the models trained using varying test site configurations are similar. This indicates that an accurate identification of active source areas in the field, even if limited to a few locations, may provide representative data to train the models. For this reason, the final model for the entire island was trained by selecting the active source areas identified in the four test sites. To improve the reliability of the modelling, the pixels considered not prone to rockfall initiation were selected in the vicinity of the mapped source areas (buffer zone), where we assumed that rockfall detachments were not present.

The final source area zonation for the entire island of El Hierro was prepared using an combination (i.e. CFM model) of various statistical supervised multivariate classification approaches (i.e. linear discriminant analysis, quadratic discriminant analysis, and logistic regression model). The probabilistic map and associated uncertainty are shown in Fig. 8. As expected, the rockfall source areas are preferentially located in areas with high slope gradients, but this factor itself is not sufficient to explain the spatial distribution on the entire island, with lithological information contributing significantly to their identification. Fig. 8 also provides the contingency and ROC plot for the CFM model training, with results that are comparable to similar configurations (Case 3 of different Scenarios). As already discussed for landslide susceptibility modelling (Rossi et al., 2010; Rossi and Reichenbach, 2016), the use of CFM, which is an ensemble of different classification approaches, has the main advantage of reducing the final modelling uncertainties.

The use of probabilistic models for source area identification provides a reliable extent and distribution of the rockfall detachment areas for the entire island, improving the completeness and representativeness of the inputs necessary for rockfall runout modelling. However, additional analyses should compare rockfall source area maps obtained using different approaches and evaluate their consequences on rockfall

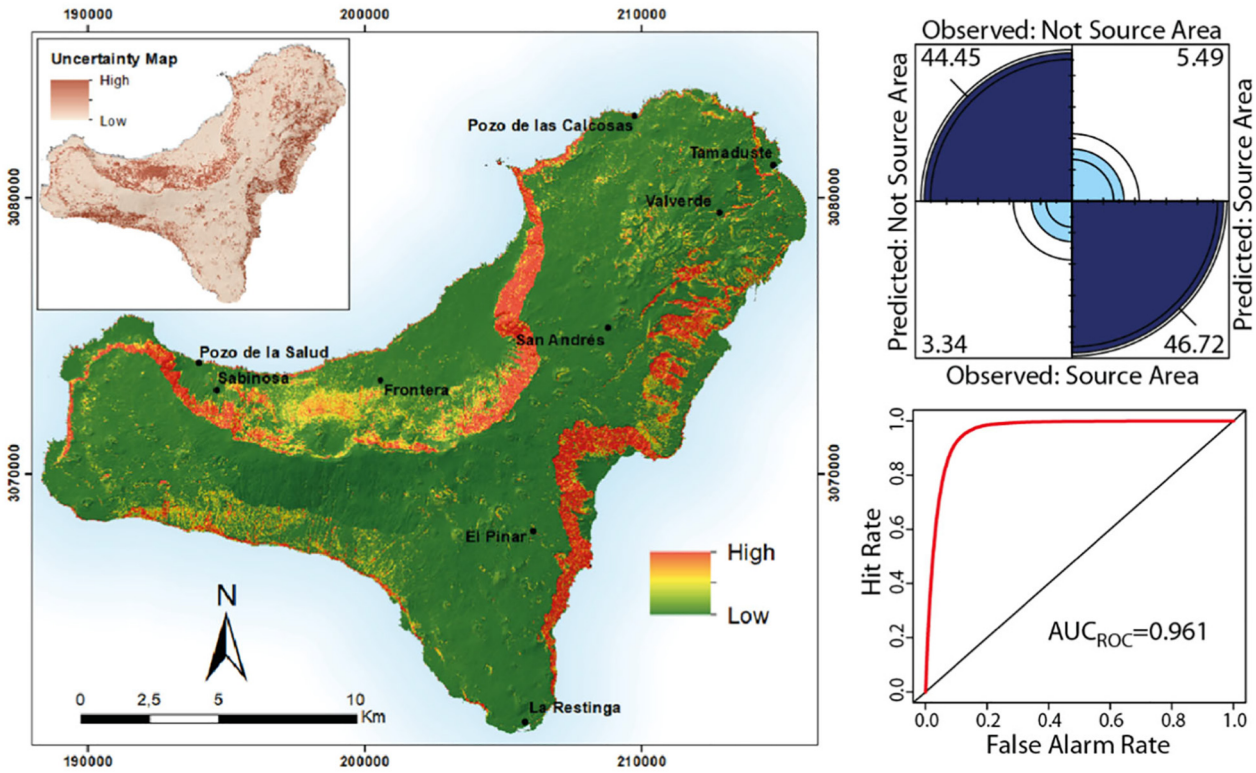

Fig. 8. Final probabilistic source areas map obtained by applying the LAND-SUITE models' ensemble/combination. The map shows the probability of the pixels being a source area, ranging from 0 (low) to 1 (high). Contingency and ROC plots for the CFM model training are shown in the figure.

runout zonation. At the regional scale, the approach proposed proved to be effective for the identification of rockfall source areas based on various geo-environmental variables.

5. Conclusion

The analysis described in this study revealed that it is possible to identify source areas using a supervised statistical classification approach with an optimal modelling configuration obtained using "active source areas" as the dependent variable (i.e. the areas where recent evidence of detachments are visible in the field) mapped in few but representative test sites. Compared with other maps derived by slope angle thresholding, the probabilistic maps may improve rockfall susceptibility zonation, providing a more objective identification of source areas by comprehensively considering the complexities of the rockfall initiation process. Potentially, these probabilistic maps could support the identification of an appropriate number of rockfall trajectories to be simulated from each source area, which is a critical parameter for rockfall runout simulation software. Future studies should evaluate and compare how rockfall source area maps obtained using different approaches affect rockfall runout modelling zonation. A probabilistic map of rockfall source areas at a regional scale can support civil protection and emergency authorities and decision makers to evaluate and assess the potential spatial distribution of rockfall impacts and can be a strategic support for rockfall warning systems. In areas with similar rockfall process characteristics, such as the other islands of the Canary archipelago, the proposed probabilistic approach should be able to provide reliable regional distributions of source areas without extensive field surveys.

CRediT authorship contribution statement

M.R. participated in the methodological design and implementation, executed modelling and analysis, and participated in manuscript writing; R.S. collected data, participated in the methodological design and implementation, executed the modelling and analysis, and participated in manuscript writing; P.R. participated in the methodological design and implementation and in manuscript writing; R.M.M. collected data and participated in the methodological design and implementation and in manuscript writing.

Declaration of competing interest

The authors declare that they have no known competing financial interests or personal relationships that could have appeared to influence the work reported in this paper.

Acknowledgements

This work was funded by i) the European Commission, Directorate-General Humanitarian Aid and Civil Protection (ECHO), through the project U-GEOHAZ (Geohazard Impact Assessment for Urban Areas), Grant Agreement No. 783169, and ii) the Salvador de Madariaga Mobility Program from the Spanish Ministry of Science, Project: 384 PRX18/00020. It was also partially supported by the University of Alicante in the framework of the Quality Improvement Grant of the PhD Program in Materials, Structures, and Soil Engineering: Sustainable Construction. We thank the anonymous reviewers for their comments and suggestions that improved the quality of the article.

References

Abellán, A., Vilaplana, J.M., Martínez, J., 2006. Application of a long-range terrestrial laser scanner to a detailed rockfall study at Vall de Núria (Eastern Pyrenees, Spain). Eng. Geol. 88, 136–148. https://doi.org/10.1016/j.enggeo.2006.09.012.

Agliardi, F., Crosta, G.B., 2003. High resolution three-dimensional numerical modelling of rockfalls. Int. J. Rock Mech. Min. Sci. 40, 455–471. https://doi.org/10.1016/S1365-1609(03)00021-2.

Agliardi, F., Crosta, G.B., Frattini, P., 2009. Integrating rockfall risk assessment and countermeasure design by 3D modelling techniques. Nat. Hazards Earth Syst. Sci. 9, 1059–1073. https://doi.org/10.5194/nhess-9-1059-2009.

Aksoy, H., Ercanoglu, M., 2006. Determination of the rockfall source in an urban settlement area by using a rule-based fuzzy evaluation. Natural Hazards and Earth System Science. https://doi.org/10.5194/nhess-6-941-2006.

Becerril, L., Galve, J.P., Morales, J.M., Romero, C., Sánchez, N., Martí, J., Galindo, I., 2016. Volcano-structure of El Hierro (Canary Islands). Journal of Maps 12, 43–52. https://doi.org/10.1080/17445647.2016.1157767.

Bechtel, B., 2016. The climate of the canary Islands by annual cycle parameters. International Archives of the Photogrammetry, Remote Sensing and Spatial Information Sciences - ISPRS Archives https://doi.org/10.5194/isprsarchives-XLI-B8-243-2016.

Carracedo, J.C., Badiola, E.R., Guillou, H., De la Nuez, J., Pérez Torrado, F.J., 2001. Geología y vulcanología de La palma y El Hierro, Canarias Occidentales. Estud. Geol. 57 (5–6), 175–273. https://doi.org/10.3989/egeol.01575-6134.

Chung, C.J.F., Fabbri, A.G., 1999. Probabilistic Prediction Models for Landslide Hazard Mapping, Photogrammetric Engineering and Remote Sensing.

Chung, C.-J.F., Fabbri, A.G., 2003. Validation of Spatial Prediction Models for Landslide Hazard Mapping. Nat. Hazards 30, 451–472. https://doi.org/10.1023/B:NHAZ.0000007172.62651.2b.

Corona, C., Trappmann, D., Stoffel, M., 2013. Parameterization of rockfall source areas and magnitudes with ecological recorders: when disturbances in trees serve the calibration and validation of simulation runs. Geomorphology https://doi.org/10.1016/j.geomorph.2013.02.001.

Crosta, G.B., Agliardi, F., Frattini, P., Lari, S., 2015. Key issues in rock fall modeling, hazard and risk assessment for rockfall protection. In: Lollino, G., Giordan, D., Crosta, G.B., Corominas, J., Azzam, R., Wasowski, J., Sciarra, N. (Eds.), Engineering Geology for Society and Territory. vol. 2. Springer International Publishing, Cham, pp. 43–58. https://doi.org/10.1007/978-3-319-09057-3_4.

Fanos, A.M., Pradhan, B., 2018. Laser scanning systems and techniques in rockfall source identification and risk assessment: a critical review. Earth Sys. Environ. https://doi.org/10.1007/s41748-018-0046-x.

Fawcett, T., 2006. An introduction to ROC analysis. Pattern Recogn. Lett. 27, 861–874. https://doi.org/10.1016/j.patrec.2005.10.010.

Fernandez-Hernández, M., Paredes, C., Castedo, R., Llorente, M., de la Vega-Panizo, R., 2012. Rockfall detachment susceptibility map in El Hierro Island, Canary Islands, Spain. Nat. Hazards 64, 1247–1271. https://doi.org/10.1007/s11069-012-0295-1.

Frattini, P., Crosta, G., Carrara, A., Agliardi, F., 2008. Assessment of rockfall susceptibility by integrating statistical and physically-based approaches. Geomorphology 94, 419–437. https://doi.org/10.1016/j.geomorph.2006.10.037.

Fullea, J., Camacho, A.G., Negredo, A.M., Fernández, J., 2015. The Canary Islands hot spot: new insights from 3D coupled geophysical–petrological modelling of the lithosphere and uppermost mantle. Earth Planet. Sci. Lett. 409, 71–88. https://doi.org/10.1016/j.epsl.2014.10.038.

Gee, M.J.R., Watts, A.B., Masson, D.G., Mitchell, N.C., 2001. Landslides and the evolution of El Hierro in the Canary Islands. Mar. Geol. 177, 271–293. https://doi.org/10.1016/S0025-3227(01)00153-0.

Guzzetti, F., Reichenbach, P., Wieczorek, G.F., 2003. Rockfall hazard and risk assessment in the Yosemite Valley, California, USA. Nat. Hazards Earth Syst. Sci. 3, 491–503. doi: https://doi.org/10.5194/nhess-3-491-2003

Guzzetti, F., Reichenbach, P., Ghigi, S., 2004. Rockfall hazard and risk assessment along a transportation corridor in the Nera Valley, Central Italy. Environ. Manag. 34, 191–208. https://doi.org/10.1007/s00267-003-0021-6.

Hernández Gutiérrez, L.E., Santamarta Cerezal, J.C., Colegio Oficial de Geólogos (Madrid), 2015. Ingeniería geológica en terrenos volcánicos: métodos, técnicas y experiencias en las islas Canarias. Ilustre Colegio Oficial de Geólogos, Madrid.

Hernández-Gutierrez, L.E.H., 2014. Caracterizacion geomecanica de las rocas volcanicas de las islas canarias. http://purl.org/dc/dcmitype/Text Universidad de La Laguna.

Hungr, O., Leroueil, S., Picarelli, L., 2014. The Varnes classification of landslide types, an update. Landslides 11, 167–194. https://doi.org/10.1007/s10346-013-0436-y.

Instituto Nacional de Estadística, 2019. Cifras de Población [WWW Document]. https://www.ine.es/jaxiT3/Tabla.htm?t=2910&L=0 accessed 5.13.20.

Jaboyedoff, M., Labiouse, V., 2003. Preliminary assessment of rockfall hazard based on GIS data. 10th ISRM Congress.

Jaboyedoff, M., Labiouse, V., 2011. Technical note: preliminary estimation of rockfall runout zones. Nat. Hazards Earth Syst. Sci. 11, 819–828. https://doi.org/10.5194/nhess-11-819-2011.

Jaboyedoff, M., Oppikofer, T., Abellán, A., Derron, M.-H., Loye, A., Metzger, R., Pedrazzini, A., 2012. Use of LIDAR in landslide investigations: a review. Nat. Hazards 61, 5–28. https://doi.org/10.1007/s11069-010-9634-2.

Jasiewicz, J., Stepinski, T.F., 2013. Geomorphons-a pattern recognition approach to classification and mapping of landforms. Geomorphology https://doi.org/10.1016/j.geomorph.2012.11.005.

Jolliffe, I.T., Stephenson, D.B., 2012. Forecast Verification: A Practitioner's Guide in Atmospheric Science. 2. Wiley-Blackwell, Chichester.

Lambert, C., Thoeni, K., Giacomini, A., Casagrande, D., Sloan, S., 2012. Rockfall hazard analysis from discrete fracture network modelling with finite persistence discontinuities. Rock Mech. Rock. Eng. https://doi.org/10.1007/s00603-012-0250-1.

Losasso, L., Jaboyedoff, M., Sdao, F., 2017. Potential rock fall source areas identification and rock fall propagation in the province of Potenza territory using an empirically distributed approach. Landslides 14, 1593–1602. https://doi.org/10.1007/s10346-017-0807-x.

Loye, A., Jaboyedoff, M., Pedrazzini, A., 2009. Identification of potential rockfall source areas at a regional scale using a DEM-based geomorphometric analysis. Nat. Hazards Earth Syst. Sci. 9, 1643–1653. https://doi.org/10.5194/nhess-9-1643-2009.

Luckman, B., 2013. 7.17 Processes, Transport, Deposition, and Landforms: Rockfall.

Martí, J., Ablay, G.J., Bryan, S., 1996. Comment on "the Canary Islands: an example of structural control on the growth of large oceanic-island volcanoes" by J.C. Carracedo. Journal of Volcanology and Geothermal Research 72, 143–149. https://doi.org/10.1016/0377-0273(95)00079-8.

Mason, S.J., Graham, N.E., 2002. Areas beneath the Relative Operating Characteristics (ROC) and Relative Operating Levels (ROL) Curves: statistical significance and interpretation. Q. J. R. Meteorol. Soc. 128 (584), 2145–2166. https://doi.org/10.1256/003590002320603584.

Mateos, R.M., García-Moreno, I., Azañón, J.M., 2012. Freeze–thaw cycles and rainfall as triggering factors of mass movements in a warm Mediterranean region: the case of the Tramuntana Range (Majorca, Spain). Landslides 9, 417–432. https://doi.org/10.1007/s10346-011-0290-8.

Mateos, R.M., López-Vinielles, J., Poyiadji, E., Tsagkas, D., Sheehy, M., Hadjicharalambous, K., Liscák, P., Podolski, L., Laskowicz, I., Iadanza, C., Gauert, C., Todorović, S., Auflič, M.J., Maftei, R., Hermanns, R.L., Kociu, A., Sandić, C., Mauter, R., Sarro, R., Béjar, M., Herrera, G., 2020. Integration of landslide hazard into urban planning across Europe. Landsc. Urban Plan. https://doi.org/10.1016/j.landurbplan.2019.103740.

Melzner, S., Rossi, M., Guzzetti, F., 2020. Impact of mapping strategies on rockfall frequency-size distributions. Eng. Geol. 272, 105639. https://doi.org/10.1016/j.enggeo.2020.105639.

Mühlenstädt, T., Kuhnt, S., 2011. Kernel interpolation. Computational Statistics and Data Analysis https://doi.org/10.1016/j.csda.2011.05.001.

Muzzillo, R., Losasso, L., Sdao, F., 2018. Rockfall source areas assessment in an area of the Pollino National Park (Southern Italy). Lecture Notes in Computer Science (Including Subseries Lecture Notes in Artificial Intelligence and Lecture Notes in Bioinformatics) https://doi.org/10.1007/978-3-319-95168-3_25.

Paredes, C., Sarro, R., Ramos, M., 2015. Estimación preliminar de los alcances por caída de bloques en la sierra de La Cabrera, Madrid, España. Revista mexicana de ciencias geológicas 32, 475–491.

Petje, U., Ribičič, M., Mikoš, M., 2005. Computer simulation of stone falls and rockfalls. AGS 45, 93–120. https://doi.org/10.3986/AGS45204.

R Core Team, 2018. R: A Language and Environment for Statistical Computing. R Foundation for Statistical Computing, Vienna, Austria.

Rossi, M., Reichenbach, P., 2016. LAND-SE: a software for statistically based landslide susceptibility zonation, version 1.0. Geosci. Model Dev. 9, 3533–3543. https://doi.org/10.5194/gmd-9-3533-2016.

Rossi, M., Guzzetti, F., Reichenbach, P., Mondini, A.C., Peruccacci, S., 2010. Optimal landslide susceptibility zonation based on multiple forecasts. Geomorphology 114, 129–142. https://doi.org/10.1016/j.geomorph.2009.06.020.

Ruiz-Carulla, R., Corominas, J., Mavrouli, O., 2015. A methodology to obtain the block size distribution of fragmental rockfall deposits. Landslides 12, 815–825. https://doi.org/10.1007/s10346-015-0600-7.

Santangelo, M., Alvioli, M., Baldo, M., Cardinali, M., Giordan, D., Guzzetti, F., Marchesini, I., Reichenbach, P., 2019. Brief communication: Remotely piloted aircraft systems for rapid emergency response: road exposure to rockfall in Villanova di Accumoli (central Italy). Nat. Hazards Earth Syst. Sci. 19, 325–335. https://doi.org/10.5194/nhess-19-325-2019.

Sarro, R., 2019. Simulación de desprendimientos rocosos para la gestión de emergencias e infraestructuras (PhD Thesis). Universidad de Alicante.

Sarro, R., Riquelme, A., García-Davalillo, J.C., Mateos, R.M., Tomás, R., Pastor, J.L., Cano, M., Herrera, G., 2018. Rockfall simulation based on UAV photogrammetry data obtained during an emergency declaration: Application at a cultural heritage site. Remote Sensing https://doi.org/10.3390/rs10121923.

Sarro, R., Mateos, R.M., Reichenbach, P., Aguilera, H., Riquelme, A., Hernández-Gutiérrez, L.E., Martín, A., Barra, A., Solari, L., Monserrat, O., Alvioli, M., Fernández-Merodo, J.A., López-Vinielles, J., Herrera, G., 2020. Geotechnics for rockfall assessment in the volcanic island of Gran Canaria (Canary Islands, Spain). Journal of Maps 16, 605–613. https://doi.org/10.1080/17445647.2020.1806125.

Sturzenegger, M., Sartori, M., Jaboyedoff, M., Stead, D., 2007. Regional deterministic characterization of fracture networks and its application to GIS-based rock fall risk assessment. Eng. Geol. 94, 201–214. https://doi.org/10.1016/j.enggeo.2007.08.002.

Toppe, R., 1987. Terrain models: a tool for natural hazard mapping. IAHS Publ. 162.

Volkwein, A., Schellenberg, K., Labiouse, V., Agliardi, F., Berger, F., Bourrier, F., Dorren, L.K.A., Gerber, W., Jaboyedoff, M., 2011. Rockfall characterisation and structural protection – a review. Nat. Hazards Earth Syst. Sci. 11, 2617–2651. https://doi.org/10.5194/nhess-11-2617-2011.